International Journal of Fluid Machinery and Systems
Vol. 5, No. 1, January-March 2012

DOI: http://dx.doi.org/10.5293/IJFMS.2011.5.1.001
ISSN (Online): 1882-9554

Original Paper

Numerical Analysis of the Influence of Acceleration on Cavitation Instabilities that arise in Cascade

Yuka Iga[1] and Tasuku Konno[2]

[1]Institute of Fluid science, Tohoku University
2-1-1 Katahira, Aoba-ku, Sendai, Miyagi, 980-8577, Japan, iga@ifs.tohoku.ac.jp
[2]Graduate School of Mechanical Engineering, Tohoku University
2-1-1 Katahira, Aoba-ku, Sendai, Miyagi, 980-8577, Japan

Abstract

In the turbopump inducer of a liquid propellant rocket engine, cavitation is affected by acceleration that occurs during an actual launch sequence. Since cavitation instabilities such as rotating cavitations and cavitation surges are suppressed during launch, it is difficult to obtain data on the influence of acceleration on cavitation instabilities. Therefore, as a fundamental investigation, in the present study, a three-blade cyclic cascade is simulated numerically in order to investigate the influence of acceleration on time-averaged and unsteady characteristics of cavitation that arise in cascade. Several cases of acceleration in the axial direction of the cascade, including accelerations in the upstream and downstream directions, are considered. The numerical results reveal that cavity volume is suppressed in low cavitation number condition and cavitation performance increases as a result of high acceleration in the axial-downstream direction, also, the inverse tendency is observed in the axial-upstream acceleration. Then, the regions in which the individual cavitation instabilities occur shift slightly to a low-cavitation-number region as the acceleration increases downstream. In addition, in a downstream acceleration field, neither sub-synchronous rotating cavitation nor rotating-stall cavitation are observed. On the other hand, rotating-stall cavitation occurs in a relatively higher-cavitation-number region in an upstream acceleration field. Then, acceleration downstream is robust against cavitation instabilities, whereas cavitation instabilities easily occur in the case of acceleration upstream. Additionally, comparison with the Froude number under the actual launch conditions of a Japanese liquid propellant rocket reveals that the cavitation performance will not be affected by the acceleration under the current launch conditions.

Keywords: Cavitation Instability, Cascade, Acceleration, Homogeneous Model, CFD

1. Introduction

In the turbopump inducer of a liquid propellant rocket engine, cavitation is affected by acceleration during an actual launch sequence. As such, the possibility exists that not only the time-averaged cavity volume but also the unsteady characteristics of the cavity will be changed due to the influence of acceleration. When the unsteady characteristics of cavitation change, the mode or occurrence region of cavitation instabilities may change. As such, there is no guarantee that the once-suppressed cavitation instabilities will not reoccur. In addition, the effect of the acceleration direction on cavitation will vary when the direction of installation of the inducer changes. In the previous LE-7 Japanese liquid propellant rocket engine, the entrance of the inducer was located on the side opposite the direction of launch. In contrast, in the current LE-7A engine, the entrance of the inducer is located on the launch direction side. Then, even for same launch sequence, cavitation is exposed to reverse acceleration in each engine. However, the influence of acceleration on cavitation instabilities has not yet been clarified because most of the cavitation instabilities are suppressed during an actual launch. Therefore, under conditions involving both acceleration and cavitation instabilities, computational fluid dynamics (CFD) is considered to be a suitable approach in such investigations.

In a previous study, we developed a numerical method for simulating cavitation that is suitable for unsteady calculation and clarified two mechanisms for break-off phenomenon of sheet cavitation in the cascade[1]. We have also reproduced three types of cavitation instabilities, namely, super-synchronous and sub-synchronous rotating cavitations and cavitation surge, which occur by different mechanisms, in a three-blade cyclic cascade, without adding a model or boundary conditions for the individual phenomena[2]. In the previous study, the occurrence conditions or propagation velocity ratio, which have been well documented based on experimental results, were reproduced qualitatively. In addition, the possibility of the suppression of cavitation instabilities by a jet flow through a slit on cascade blades was reported[3]. Furthermore, we have classified three types of cavitation surges in cascade and the frequency characteristics of the cavitation surges [4] and have suggested a mechanism for the propagation

Received September 5 2011; revised October 19 2011; accepted for publication December 12 2011: Review conducted by Prof. Jun Matsui. (Paper number O11015J)
Corresponding author: Yuka Iga, Assistant Professor, iga@ifs.tohoku.ac.jp

direction of rotating cavitations in cascade [5]. The numerical method developed previously by present authors has been confirmed to be applicable to numerical simulation of cavitation instabilities.

In the present study, first, as fundamental research, the influence of acceleration on time-averaged and unsteady characteristics of cavitation is analyzed through numerical simulation of a three-blade cascade. The acceleration is adapted to the axial upstream and downstream directions. Based on the numerical results, the time-averaged cavity volume and head performance, the cavitation performance of the cascade, the occurrence conditions of cavitation instabilities, and the unsteady characteristics of the cavitation instabilities are examined. In addition, proper installation of the inducer so as to prevent cavitation instabilities is discussed.

2. Numerical Method for Simulation of a Cavitating Flow

2.1 Locally Homogeneous Model for a Compressible Gas-Liquid Two-phase Medium

In the present study, a locally homogeneous model of a compressible gas-liquid two-phase medium [1] was used for the numerical simulation of cavitation. In this model, by considering a gas-liquid two-phase field as a pseudo-single phase medium, the Navier-Stokes (N-S) equations for a continuum can be applied to a cavitating flow field in which there is discontinuity between the gas and liquid phases. The governing equations for the gas-liquid medium are the following compressible gas-liquid N-S equations:

$$\frac{\partial \mathbf{Q}}{\partial t}+\frac{\partial(\mathbf{E}-\mathbf{E}v)}{\partial x}+\frac{\partial(\mathbf{F}-\mathbf{F}v)}{\partial y}=\mathbf{S} \quad ,$$

$$\mathbf{Q}=\begin{pmatrix}\rho\\ \rho u\\ \rho v\\ \rho Y\end{pmatrix},\quad \mathbf{E}=\begin{pmatrix}\rho u\\ \rho u^2+p\\ \rho uv\\ \rho uY\end{pmatrix},\quad \mathbf{F}=\begin{pmatrix}\rho v\\ \rho uv\\ \rho v^2+P\\ \rho vY\end{pmatrix},\quad \mathbf{E}v=\begin{pmatrix}0\\ \tau_{xx}\\ \tau_{yx}\\ 0\end{pmatrix},\quad \mathbf{F}v=\begin{pmatrix}0\\ \tau_{xy}\\ \tau_{yy}\\ 0\end{pmatrix},\quad \mathbf{S}=\begin{pmatrix}0\\ a_x\\ a_y\\ \Gamma\end{pmatrix}, \tag{1}$$

where ρ, p, u, and v are the density, static pressure, and velocities of the mixture phase, and Y is the mass fraction of the gas phase. In the present study, the working fluid is water at room temperature, in which the temperature distribution is vanishingly small. Then, in order to reduce the computational load, an isothermal field at 293.15 K is assumed, and the energy conservation equation is omitted in the governing equations given in Eq. (1). The terms a_x and a_y in source term vector **S** are acceleration terms, and Γ in **S** represents the evaporation speed by the instantaneous equilibrium evaporation model[3]. Since empirical constants for evaporation speed are not necessary, the evaporation model is robust for pressure wave propagation with a rapid pressure jump accompanied by a pulsation phenomenon. Therefore, this model can be applied without distinguishing between the flow fields that experience or do not experience a cavitation surge or other phenomena.

The governing equations of Eq. (1) are closed by the equation of state for a locally homogeneous compressible gas-liquid two-phase medium. The equation of state is derived as follows by the assumption of local equilibria of pressure and temperature between the gas and liquid phases and the assumption of a linear combination of the mass of the liquid phase with the gas phase, where the liquid phase is compressible and the gas phase is considered to be an ideal gas:

$$\rho=\frac{p(p+p_c)}{K_l(1-Y)p(T+T_c)+R_gY(p+p_c)T} \quad , \tag{2}$$

where K_l is the liquid constant, R_g is the gas constant, and p_c and T_c are the pressure and temperature constants of the liquid, respectively. The speed of sound of the two-phase medium derived from Eq. (2) has been verified using experimental data for not only pure liquid and gas conditions but also the mixed gas-liquid condition [1]. The present compressible numerical approach is then considered to be applicable to the numerical simulation of mutual interference between cavitation and a fluid machinery system.

In this numerical method, since the cavity surface, which is a discontinuity in density, is described as the gradient of the void fraction, a numerical method for a contact discontinuity problem in compressible fluid can be used. As such, the cavity form is not restricted. At the same time, the thickness of the cavity surface depends on the resolution of the computational mesh. Therefore, this numerical method is considered to be applicable to the numerical analysis of a wide range of cavitation conditions, with the exception of incipient cavitation.

2.2 Numerical Scheme

In the present study, the governing equations of Eq. (1) are solved using the finite difference method. Since it is necessary to stably simulate the discontinuities of the large density jump at the gas-liquid interface in a cavitating flowfield, the total variation diminishing (TVD) scheme is used in order to ensure the monotonicity of the solution. Specifically, the explicit TVD-MacCormack scheme [6] with second-order accuracy in time and space is used.

The present numerical method has been validated for the time-averaged pressure distribution on a cascade blade with several angles of attack under non-cavitation conditions [1]. Mesh convergence has been examined [5] for a single hydrofoil under non-cavitation and cavitation conditions in calculations with and without a turbulence model, i.e., the RANS model (Baldwin-Lomax model with Degani-Schiff modification). In addition, the unsteady characteristics of sheet cavitation in a single hydrofoil have been validated [5] through calculations with and without the RANS model. The RANS calculation has been shown to be applicable to a non-cavitating flow field, while not contributing to unsteady cavitation, which is the objective of the present study. In the literature, it has often been reported that excess viscosity around termination of a sheet cavity prevents unsteadiness of the cavity when a RANS model for single-phase flow is used. Therefore, a modified method in which the excess viscosity is decreased in a two-phase condition has been developed [7] and applied [7-11]. However, this modified method is still not sufficient. Therefore, no

turbulence model was applied in the present study because no reliable turbulence model for studying the characteristics of oscillation in cavitation instabilities exists. Moreover, this reduces the computational load. However, a macroscopic disturbance in the flow field, which is caused by oscillation of the cavity volume, was resolved by the proposed numerical method without the use of the turbulence model.

2.3 Computational Condition

The target flow field of the present study was a three-blade cyclic flat-plate cascade, as shown in Fig. 1, in which the solidity is $C/h = 2.0$, the stagger angle is $\gamma = 75°$, and the blade thickness is zero. In the present study, the simplest configuration, e.g., a flat plate with no thickness, was selected for the target blade, which is accompanied by an apparent separation point because no turbulence model was used. The upstream area was two chord lengths from the inlet boundary to the leading edge of the blade, and the downstream area was three chord lengths from the trailing edge to the outlet boundary. One cascade passage had 261 x 71 mesh points. A non-slip condition was assumed on the wall boundary of the blades, and a cyclic boundary condition was imposed at every three cascade passages in order to reproduce the circumferential instabilities in a cascade, such as rotating cavitation. In the inlet boundary, constant conditions of flow angle, total pressure, and void fraction were applied, where static pressure was extrapolated, and velocity was calculated from the condition of constant total pressure. In the outlet boundary, a constant-static-pressure condition was applied, and the velocity and density were extrapolated.

In the present study, the acceleration a [m/s^2] is imposed in the axial direction, and the axial downstream direction is assumed to be positive. Eight conditions of acceleration are imposed, as shown in Table 1, where G is gravitational acceleration, which is assumed to be 9.8 m/s^2. The terms a_x and a_y in the source term vector **S** in the governing equations of Eq. (1) represent source terms, which are due to the acceleration, $a_x = a \cos\gamma$ and $a_y = -a \sin\gamma$, in the present study.

Table 1 Acceleration and Froude number

Acceleration a [m/s^2]	5G	3G	1G	0.1G	0G	– 0.1G	– 1G	– 3G
Froude number Fr	4.28	5.52	9.56	30.2	Inf.	30.2	9.56	5.52

In all cases, the inflow angle was set at $\alpha_{in} = 7°$, and the inflow velocity was approximately $U_{in} = 12$ m/s. Computation was performed for several cavitation numbers σ at each acceleration condition, where σ is controlled by changing the outlet static pressure. The cavitation number σ, Froude number Fr, flow rate coefficient ϕ, head coefficient H, and the propagation velocity ratio of rotating cavitation PVR were estimated as follows:

$$\text{Cavitation number: } \sigma = \frac{(p_{in} + \rho_{in} a(2C\cos\gamma)) - p_v}{1/2\rho_{in} U_t^{\,2}}, \tag{5}$$

$$\text{Froude number: } \mathrm{Fr} = U_t / \sqrt{3ha}, \tag{6}$$

$$\text{Flow rate coefficient: } \phi = U_a / U_t, \tag{7}$$

$$\text{Head coefficient: } H = \frac{U_{a2} - U_{a1}}{U_t^{\,2}} + \frac{2(p_2 - p_1)}{\rho_{in} U_t^{\,2}} + \frac{2a(x_2 - x_1)(-\cos\gamma)}{U_t^{\,2}}, \tag{8}$$

$$\text{Propagation velocity ratio: } PVR = \frac{U_t + U_{cav}}{U_t}, \tag{9}$$

where U_t and U_a are the circumferential and axial velocities of U_{in}, respectively. Here, U_{cav} is the velocity of the apparent circumferential propagation of the uneven cavity volume in rotating cavitation. Subscript *in* indicates the inlet boundary of the computational domain, and subscripts *1* and *2* indicate locations 1 *C* upstream from the cascade entrance and 1*C* downstream from the cascade exit, respectively. Here, σ corresponds local cavitation number in cascade inlet, which is estimated by adding potential head from inlet boundary to cascade inlet to static pressure in inlet boundary. The σ and ψ were calculated from time-averaged computational results for each case. The angles of attack $\alpha_{in} = 7°$ correspond to $\phi = 0.141$. The *Fr* of each acceleration is shown in the lower row of Table 1.

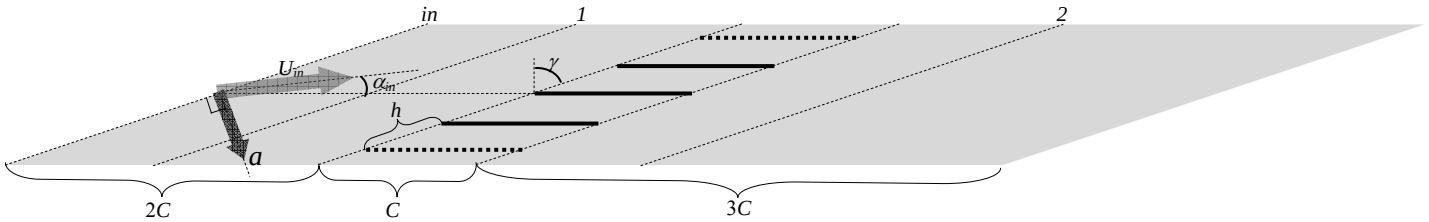

Fig. 1 Schematic diagram of the three-blade cyclic flat-plate cascade of the present study ($C/h = 2.0$, $\gamma = 75°$)

3. Results and Discussion

3.1 Cavity volumes and the aspects of the cavitation

In the present study, calculations are performed using various cavitation numbers σ in each acceleration field. Based on the

numerical results, the time-averaged cavity volume was estimated, and the results are shown in Fig. 2. Here, the cavity region is assumed to be a region in which the void fraction exceeds 0.01. In addition, the approximated curve of each acceleration field is shown in Fig. 2. In the figure, it is shown that the difference of time-averaged cavity volumes is not seen in the region where σ is over 0.2, but that can be seen at higher acceleration fields in the region where σ is under 0.2. In the region, the time-averaged cavity volumes decrease at a = 3G and 5G which are higher acceleration in downstream direction in the present study, on the other hand, that increases at a = – 3G which is higher upstream-acceleration. It indicates that the acceleration in the axial upstream direction promotes the development of cavitation, and acceleration in the axial downstream direction suppresses the development of cavitation. Because the σ which is horizontal axis of Fig. 2 corresponds time-averaged local cavitation number in cascade inlet, time-averaged static pressure in cascade inlet takes same value in each case when the σ takes same value. Therefore, the difference of time-averaged cavity volumes between in each acceleration in lower σ region is considered to be yielded by following two reasons: one is the difference of static pressures in cascade outlet, the other is the bending effect of acceleration on streamline which was reported before by theoretical analysis of acceleration gravity effects on characteristics of supercavitating hydrofoil [12]. In addition, in the acceleration fields of 5G and 3G, the cavity volume continues to increase at σ is about 0.05. At that time, σ reaches zero in inlet boundary of computational domain. This means that the region inside the cascade is not filled by cavitation when the upstream pressure becomes saturated at vapor pressure, i.e., part of the cavity that occurs upstream is believed to condensate or contract while flowing to cascade as a consequence of the potential head in the higher acceleration fields of 5G and 3G.

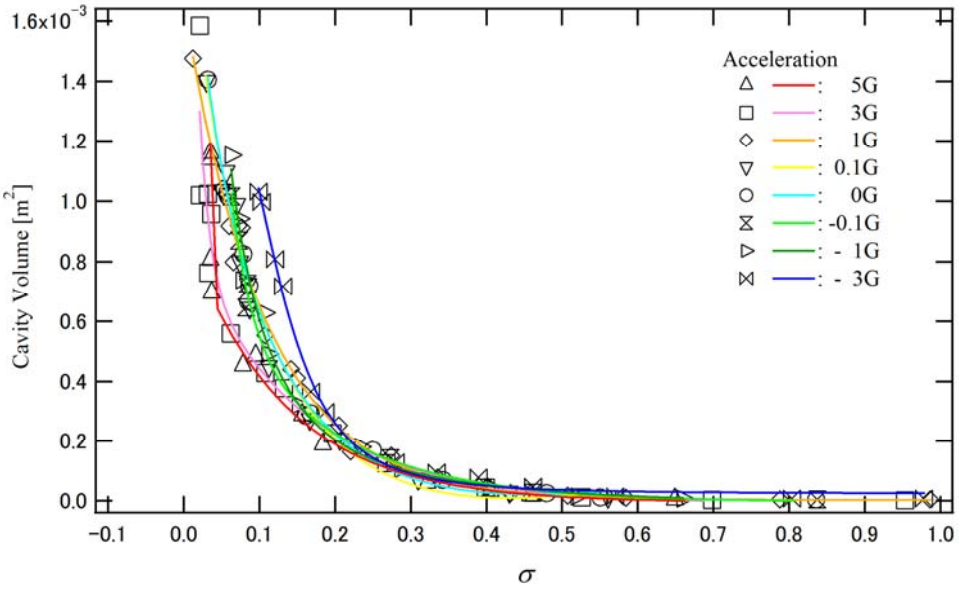

Fig. 2 Time-averaged cavity volume in the present three-blade cyclic cascade

Next, the aspects of cavitation in each acceleration field are compared. In Fig. 3, the time evolutions of the void fraction distribution are shown for accelerations of a = -3G (Fig. 3(a)), 0.1G (Fig. 3(b)), and 3G (Fig. 3(c)). In these cases, σ is approximately 0.1, the difference of time averaged cavity volumes appears in around the σ region. As shown in the figures, the instantaneous sheet cavity length is obviously long at a = – 3G. Although the maximum sheet cavity length is longer at a = 3G than that at a = 0.1 G, averaged cavity length is considered to be shorter conversely because very small cavity occurs on a blade when a sheet cavity fully develops on the other blade. Because the time-averaged cavity volumes are different even though the cavitation numbers are close in the three cases in Fig. 3, arising types of cavitation instabilities are different. Specifically, rotating-stall cavitation occurs in Fig. 3 (a), cavitation surge occurs in (b), and super-synchronous rotating cavitation occurs in (c). Thus, a difference of the instantaneous aspects of cavitation can be seen in each case. In rotating type instabilities which is rotating-stall cavitation and rotating cavitation shown in Fig. 3 (a) and (c), three sheet cavities oscillate discretely in each three blade. The cavities break in an order of Blade 1 – 2 – 3 in rotating-stall cavitation, that breaks in an order of Blade 3 – 2 – 1 in super-synchronous rotating cavitation. In contrast, in cavitation surge shown in Fig. 3 (b), three sheet cavities oscillate simultaneously in each blade.

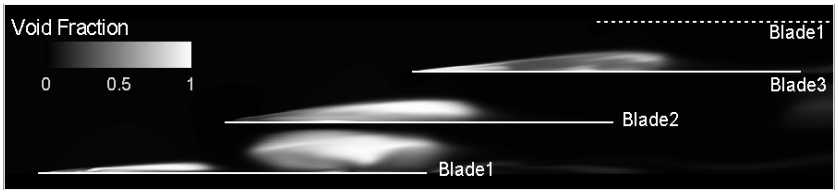

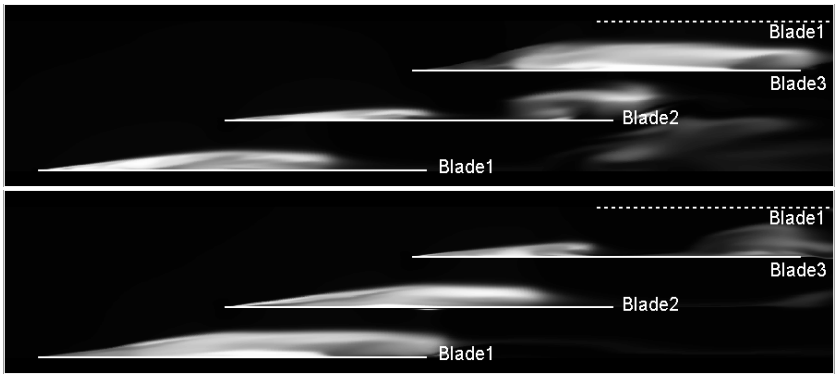

(a) $a = -3\mathrm{G}$ m/s^2 ($\sigma = 0.103$, $H = 0.217$, time interval = 12.8 ms)

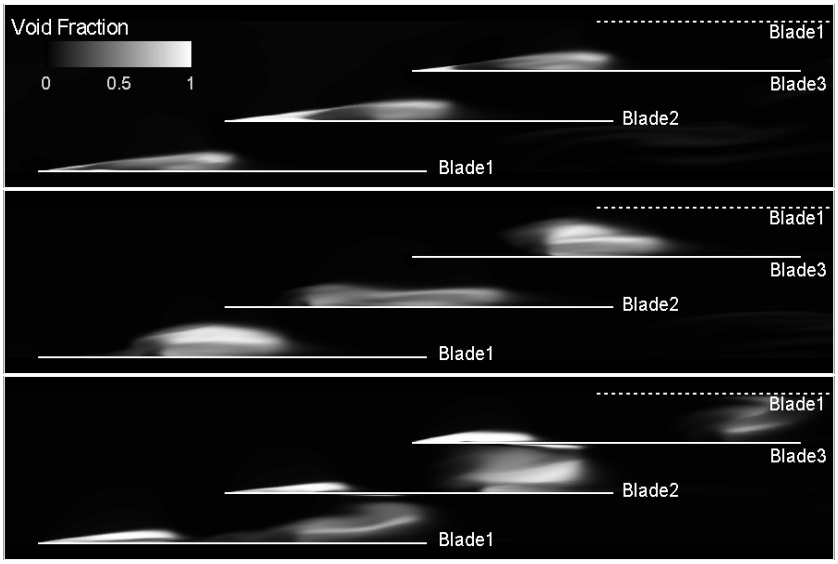

(b) $a = 0.1\mathrm{G}$ m/s^2 ($\sigma = 0.112$, $H = 0.365$, time interval = 9 ms)

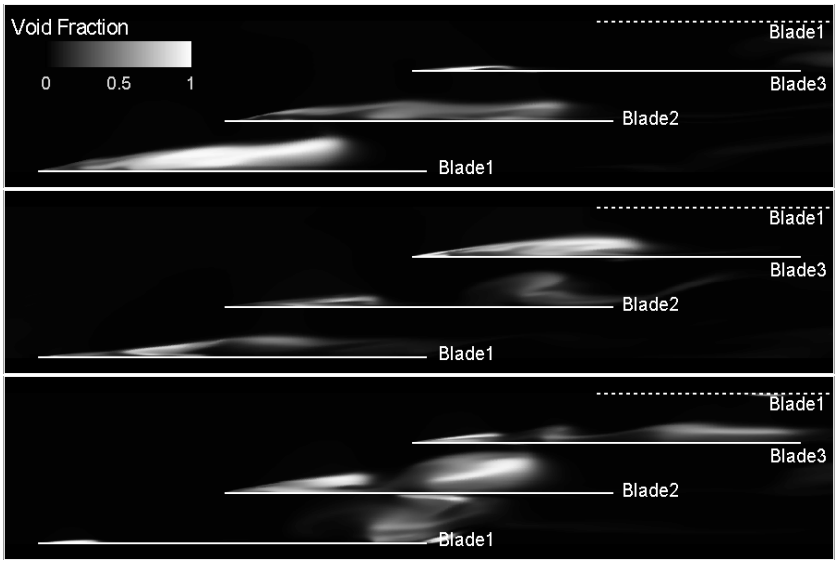

(c) $a = 3\mathrm{G}$ m/s^2 ($\sigma = 0.108$, $H = 0.355$, time interval = 16 ms)

Fig. 3 Time evolution of the void fraction distribution at each acceleration

3.2 Time-averaged head performance

The time-averaged head coefficient H is estimated in each case, as shown in Fig. 4, which also shows the approximated curves in each acceleration field. As shown in this figure, there is also difference in the head coefficient at higher σ region where no cavitation occurs. The potential head by acceleration has been compensated as shown in Eq. (8). Then the difference in the head comes from other than the change of static pressure by acceleration. In the previous literature [12] referred before, it was reported that not only static pressure but also streamline changes in an acceleration field. Then the deceleration effect of the present cascade is considered to change in each acceleration field. In the present study, the stream line is considered to be bended to the

direction of acceleration and the apparent camber appears, then, the head in higher σ region is considered to increase in acceleration in the axial-downstream direction.

As σ decreases, a head drop is observed for all accelerations, where the head coefficient suddenly decreases at a certain value of σ. A head drop occurs when the cavity develops and blocks off the throat, and a low head drop σ indicates high cavitation performance. Figure 4 shows that, for acceleration in the axial-upstream direction a = – 3G, the head drop σ value shifts to the higher σ side. Therefore, it is confirmed that the cavitation performance of the cascade decreases when higher acceleration acts in the axial-upstream direction. Additionally, at the higher acceleration in axial-downstream direction a = 5 G and 3 G, the heads drop moderately. That is because development of cavitation is suppressed by the axial-downstream acceleration around the head-drop region as described before in Fig. 2.

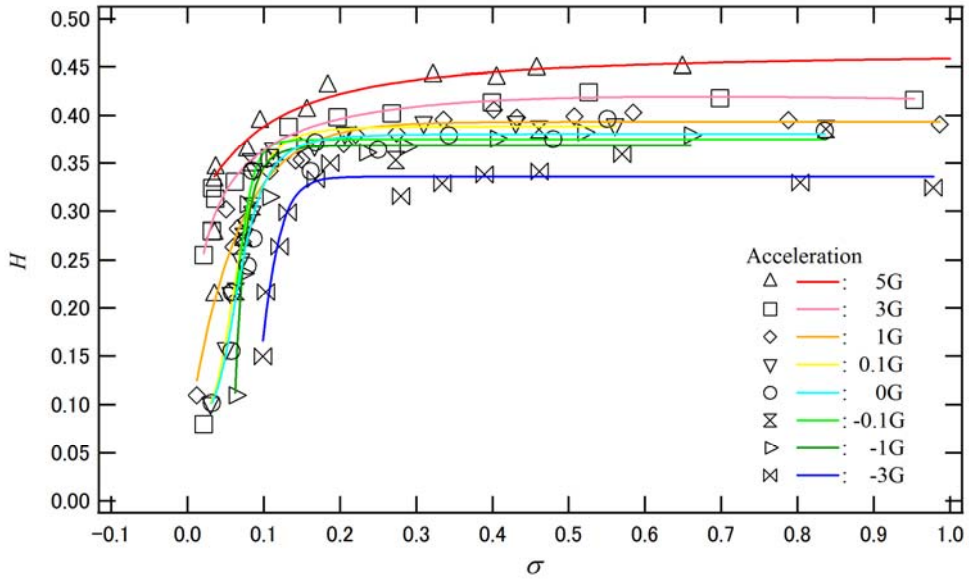

Fig. 4 Time-averaged head performance of the present three-blade cyclic cascade at each acceleration

Next, the σ value corresponding to a 30% head drop is estimated from the approximated curves for each acceleration in Fig. 4, and its dependence on the Froude number Fr is shown in Fig. 5. Although, in industry, the cavitation performance of pumps is generally discussed at the 3% drop point, a larger value of 30% is used in the present study because there is insufficient data for the 3% head drop point and the accuracy of the approximation is not so high. Also, the cavitation performance from a = – 3 G to 3 G are shown in Fig. 5, because 30 % drop point could not be detected in the approximated curve for 5 G in Fig. 4. The vertical axis of Fig. 5 is reversed. Thus, the cavitation performance is better when the plots are located at a higher position along the vertical axis. In Fig. 5, the cavitation performance increases with increasing in acceleration in axial-downstream direction as 3 G, and decreases with increasing of that in axial-upstream direction as -3 G. For reference, the minimum Froude numbers during the actual launch sequence of a Japanese liquid propellant rocket are indicated by arrows along the horizontal axis of Fig. 5, as calculated for an acceleration of 6G m/s^2, a diameter of inducer of 0.08 m, and a rotating speed of 42,000 rpm in the liquid hydrogen pump (LH2) and 18,300 rpm in the liquid oxygen pump (LOX). As shown in this figure, within the range of the Fr number in the current launch conditions, the cavitation performance is not affected by the acceleration. At the same time, on the unseen occasion such as superposition of maximum acceleration with heavy cavitation surge, Fig. 5 indicates the possibility of decrease of cavitation performance in the acceleration imposed in axial-upstream direction.

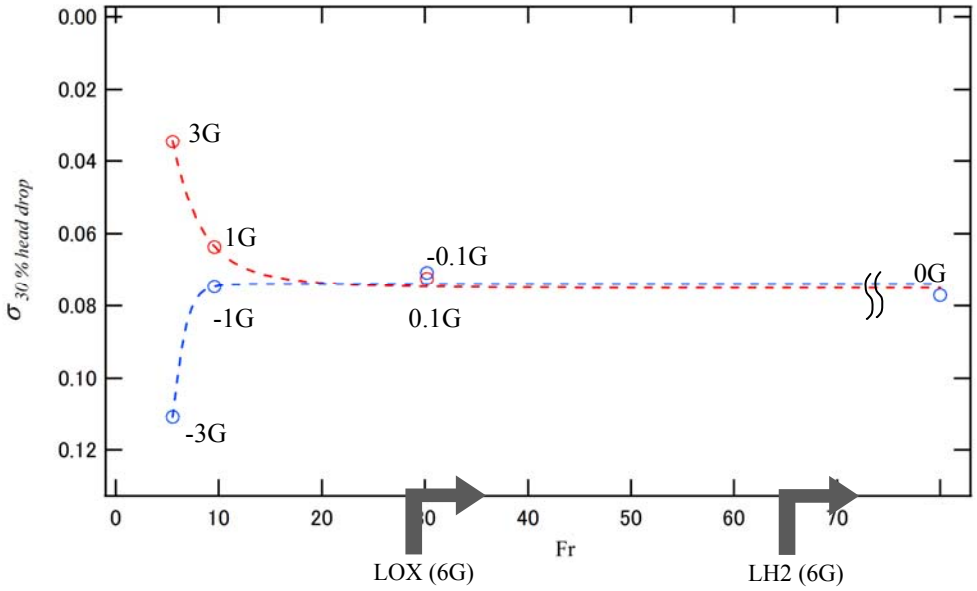

Fig. 5 Variation of 30% head drop σ in each acceleration field

3.3 Cavitation instabilities

The occurrence of cavitation instabilities is detected in each case, and an occurrence map is generated, as shown in Fig. 6, which relates the acceleration (vertical axis) and the cavitation number (horizontal axis). The occurrence of cavitation instabilities is judged by waveforms of variation monitored for upstream pressure, upstream flow rate, and cavity volume, as well as the aspects of the flow field. In Fig. 6, in lower acceleration condition a = 0.1 G to – 0.1 G, cavitation surge type 1 (Type 1 C.S), super-synchronous rotating cavitation (Super-S R.C), cavitation surge type 2 (Type 2 C.S), and sub-synchronous rotating cavitation (Sub-S R.C) occur in turn according to the decrease of σ. For another acceleration filed, in the region $\sigma >$ 0.2 where time averaged cavity volume is almost same in each acceleration in Fig. 2, same type of cavitation instabilities arises in same σ condition. On the other hand, in low σ region under 0.2, the occurrence limit and arising type of each cavitation instabilities changes because the cavity volume changes at the higher accelerations in the axial-upstream and downstream directions. Regarding the occurrence limit, the occurring σ regions of each cavitation instabilities move collectively to a lower-σ region according to the increase in acceleration in the axial-downstream direction, although the change is small. Regarding the type of instabilities, at a = 5G, which is the largest acceleration in the present study, sub-synchronous rotating cavitation (Sub-S R.C.) is not observed. Sub-S R.C. is known to occur generally in low-σ regions [13, 14]. In this study, the maximum cavity volume appearing at 5G is larger than that for the case in which Sub-S R.C occurs at other accelerations. In addition, rotating cavitations are known to be caused by choking of the throat or interference between cavity termination and the leading edge of the neighboring blade, which was reported in a inducer [15] and a centrifugal pump [16]. Therefore, the choking or interference is thought to be suppressed by the cavity thinning or cavity oscillation in the direction of diminishing thickness due to the influence of higher axial-downstream acceleration. Then, Sub-S R.C. is suppressed in the lower-σ region. On the other hand, at a = -3G, rotating-stall cavitation (R-stall C) occurs in some cases in the relatively high-σ region around σ = 0.15. In our previous study, we verified that R-stall C occurs at a high-angle-of-attack, low-flow-rate condition [5]. Therefore, the cavity thickness or the oscillation in the thickness direction is thought to be promoted by the influence of axial upstream acceleration, and the flow field becomes similar to that of a high-angle-of-attack condition. Therefore, the acceleration in the axial-downstream direction is shown to be robust against the occurrence of circumferential cavitation instabilities. In contrast, circumferential cavitation instabilities occur easily in the case of acceleration in the axial-upstream direction. Therefore, it can be summarized that it is advantageous to install the inducer such that the entrance is facing the launch direction of the rocket.

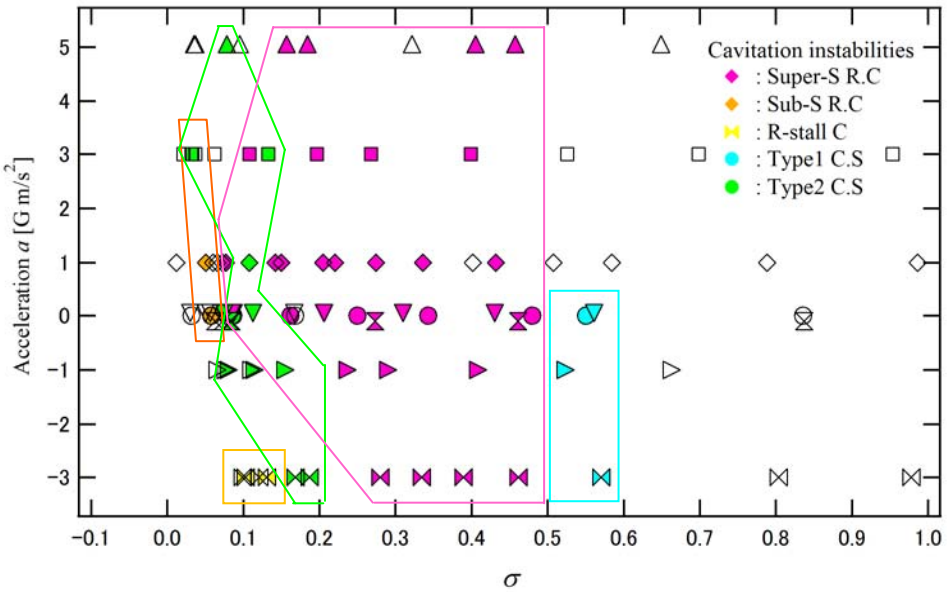

Fig. 6 Occurrence map of cavitation instabilities of the present three-blade cyclic cascade at each acceleration

3.4 Oscillating characteristics of cavitation instabilities

Propagation velocity ratios of circumferential instability, such as Super-S R.C., Sub-S R.C., and R-stall C., are estimated as shown in Fig. 7. The propagation velocity ratio (*PVR*) is expressed by Eq. (9), which indicates the apparent propagation velocity of an uneven cavity volume in an absolute coordinate system, assuming that the cascade is rotating. Then, *PVR* = 1 indicates that the uneven cavity volume attaches to the blade and does not propagate. In addition, *PVR* > 1 indicates that the uneven cavity volume propagates in the rotating direction of cascade, and *PVR* < 1 indicates that the uneven cavity volume propagates in the opposite rotating direction of cascade in the relative coordinate system, which is anchored on the cascade blade. The *PVR*s for each acceleration are shown together in Fig. 7, which indicates that the *PVR* does not change in each acceleration field. According to a propagation mechanism proposed by the authors [5], the *PVR* depends on the rotating stall speed, which is primarily affected by the fluid inertia force inside a cascade. In the present study, acceleration is applied in the axial direction, and the circumferential inertia force is not affected by the acceleration. Therefore, the resulting *PVR* does not change for each acceleration.

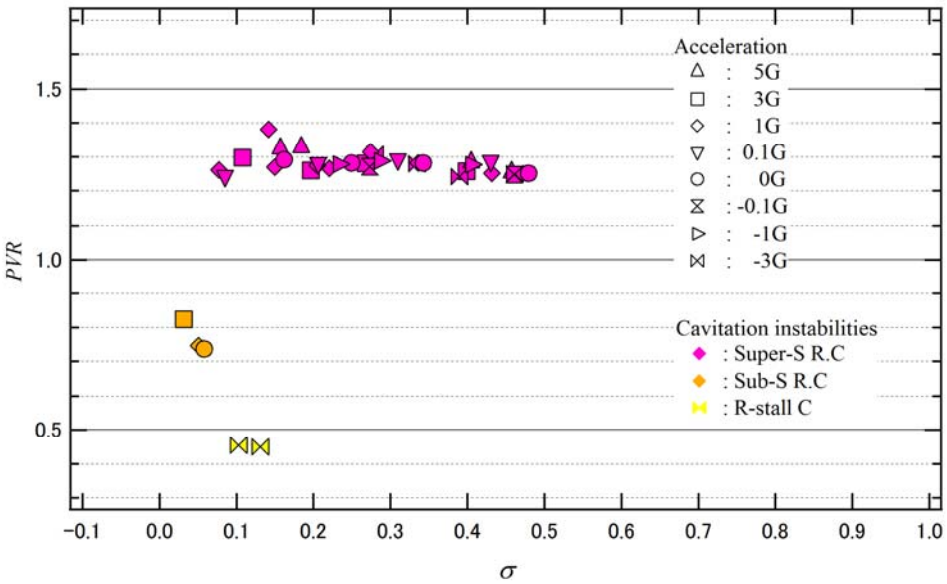

Fig. 7 Propagation velocity ratio of rotating cavitations in the three-blade cyclic cascade

Next, the frequencies of the cavitation surge, which is an axial instability, are estimated, as shown in Fig. 8. Here, the frequency f is transformed into a non-dimensional value by division by the rotating frequency of cascade f_0. In our previous study, cavitation surge occurring in cascade was classified into three types [4], two of which occurred in the present study. The first type is Type 1 C.S., which corresponds to normal surging oscillation without cavitation, the frequency of which does not change with the change in σ and occurs accompanied by vortex cavitation in the shear layer in our calculation of cascade. The second type is Type 2 C.S., which corresponds to the usual cavitation surge, the frequency of which decreases according to the decrease in σ and occurs accompanied by sheet cavitation in our calculation of cascade. In Fig. 8, the frequencies of Type 1 C.S are constant at each acceleration, and acceleration does not affect the oscillation characteristics in surging oscillation. On the other hand, in Type 2 C.S, although there is insufficient data for each acceleration, the gradient of the frequency appears to become gradual with increasing in acceleration in the axial-downstream direction. Cavitation surge can be explained as one-dimensional oscillation of a spring-mass system. In the present study, the acceleration in the axial direction may affect the vibration properties of the spring-mass system. As such, the gradient of cavitation surge frequency changes in each acceleration field.

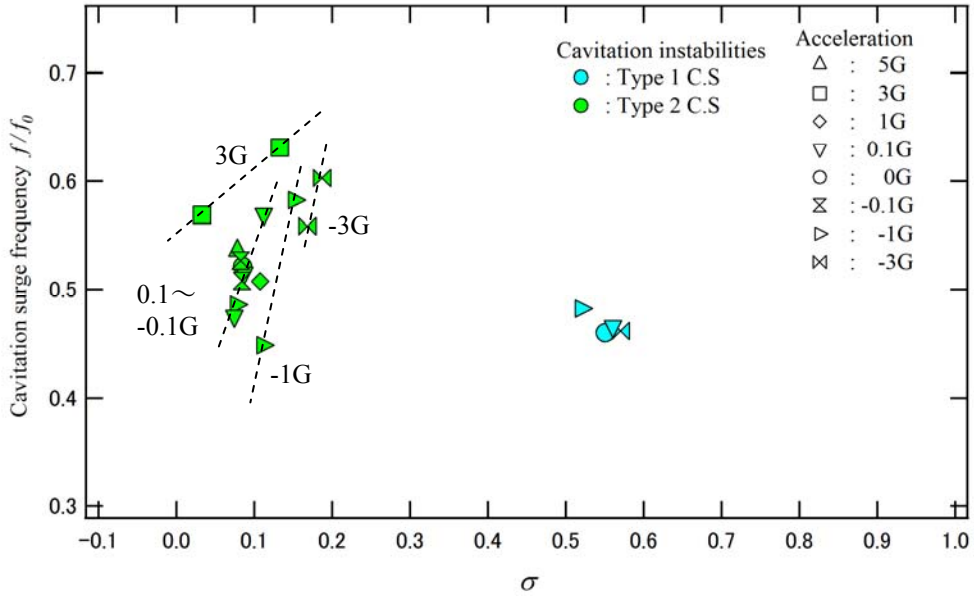

Fig. 8 Surge frequency occurring in the three-blade cyclic cascade

4. Conclusion

In the present study, as fundamental research, the influence of acceleration on the time-averaged and unsteady characteristics of cavitation was first analyzed through numerical simulation of a three-blade cascade. The results are summarized as follows.

The present study revealed that the time-averaged cavity volume and instantaneous cavity length are suppressed by high axial-downstream acceleration, but are advanced by high axial-upstream acceleration, both in low cavitation number region. Then, the

cascade head drops moderately at the high axial-downstream acceleration, and the head drop σ value shifts to the higher σ side, which means a decrease in cavitation performance, at high axial-upstream acceleration.

The cavitation performance of the cascade was shown not to be affected by the acceleration in the current launch condition of the liquid-propellant rocket.

The occurrence regions of the cavitation instabilities move collectively to a low-cavitation-number region with increasing in the acceleration in axial-downstream direction in low cavitation number condition. although the change is small. Also, it is shown that the acceleration in the axial-downstream direction is predicted to be robust against circumferential cavitation instabilities, such as rotating cavitations and rotating-stall cavitation, whereas the circumferential instabilities occur easily in the case of acceleration in the axial-upstream direction. Therefore, it is better to install the inducer such that the entrance is facing the launch direction of the liquid propellant rocket.

In the present acceleration field in the axial direction, the oscillating characteristics of circumferential instability are not affected by the acceleration, whereas the oscillating characteristics of axial instability, such as cavitation surge, change in each acceleration field.

References

[1] Iga, Y., Nohmi, M., Goto, A., Shin, B. R., and Ikohagi, T., 2003, "Numerical Study of Sheet Cavitation Break-off Phenomenon on a Cascade Hydrofoil," J. Fluids Eng., Trans. ASME, Vol. 125, No. 4, pp. 643-651.

[2] Iga, Y., Nohmi, M., Goto, A., and Ikohagi, T., 2004, "Numerical Analysis of Cavitation Instabilities Arising in The Three-Blade Cascade," J. Fluids Eng., Trans. ASME, Vol. 126, No. 3, pp. 419-429.

[3] Iga, Y., Hiranuma, Y. Yoshida, T., Ikohagi. T., 2008, "Numerical Analysis of Cavitation Instabilities and the Suppression in Cascade," Journal of Environment and Engineering, Vol. 3, No. 2, pp. 240-249.

[4] Iga, Y., Hashizume, K., Yoshida, Y., 2011, "Numerical Analysis of Three Types of Cavitation Surge in Cascade," Journal of Fluids Engineering, Trans. ASME, Vol. 133, Issue 7, 071102-1 – 071102-13.

[5] Iga, Y., Yoshida, Y., 2011, "Mechanism of Propagation Direction of Rotating Cavitations in a Cascade," Journal of Propulsion and Power, Vol. 27, No. 3, pp. 675-683.

[6] Yee, H. C., 1987, "Upwind and Symmetric Shock-Capturing Schemes," NASA-TM, 89464.

[7] Delgosha, O. C., Patella. R. F., and Reboud, J. L., 2003, "Evaluation of the Turbulence Model Influence on the Numerical Simulations of Unsteady Cavitation," J. Fluids Eng., Trans. ASME, 125, pp. 38-45.

[8] Giorgi, M. G. D., Ficarella, A., and Laforgia, D., 2005, "Comparison of Different Physical Models for the Simulation of Cavitating Flow Around a Hydrofoil," Proc. ASME FEDSM, Paper No. FEDSM2005-77142.

[9] Zhou, L., and Wang, Z., 2008, "Numerical Simulation of Cavitation Around a Hydrofoil and Evaluation of a RNG k-w Model," J. Fluids Eng., Trans. ASME, 130, pp. 011302-1-011302-7.

[10] Li, D-Q., Grekula, M., and Lindell, P., 2009, "A Modified SST k- Turbulence Model to Predict the Steady and Unsteady Sheet Cavitation on 2D and 3D Hydrofoils," Proc. The 7th Int. Symp. On Cavitation CAV2009, Michigan, Paper No. 107.

[11] Seo, J. H., and Lele, S. K., 2009, "Numerical Investigation of Cloud Cavitation and Cavitation Noise on a Hydrofoil Section," Proc. The 7th Int. Symp. On Cavitation CAV2009, Michigan, Paper No. 62.

[12] Oba, R., and Ito, Y., 1971, "Gravity Effects on Characteristics of Supercavitating Hydrofoils (Report 2, Case of Steady Longitudinal Acceleration Gravity)" Rep. Inst. High Speed Mech. Japan, Vol. 24, pp. 47-64.

[13] Tsujimoto, Y., Yoshida, Y., Maekawa, Y., Watanabe, S., and Hashimoto, T., 1997, "Observations of Oscillating Cavitation of an Inducer," J. Fluids Eng., Trans. ASME, Vol. 119, pp. 775-781.

[14] Goirand, B., Collongeat, L., Dutertre, A., Morel, Ph., 2002, "Vinci Fuel Turbopump Testing Activity Achievements," Proc. 4th International Conference on Launcher Technology "Space Launcher Liquid Propulsion," Belgium, No. 146.

[15] Horiguchi, H., Watanabe, S., Tsujimoto, Y., 2000, "Theoretical Analysis of Cavitation in Inducers with Unequal Blades with Alternate Leading Edge Cutback: Part I – Analytical Methods and the Results for Smaller Amount of Cutback," J. Fluids Eng., Trans. ASME, Vol. 122, pp. 412-418.

[16] Friedrichs, J., Kosyna, G., 2002, "Rotating Cavitation in a Centrifugal Pump Impeller of Low Specific Speed, " J. Fluids Eng., Trans. ASME, Vol. 124, pp. 356-362.